

Antiferromagnetism beyond classical percolation threshold in the site-diluted half-filled one-band Hubbard model in three dimensions

Sourav Chakraborty¹, Anamitra Mukherjee^{2,*}, Kalpataru Pradhan^{1,†}

¹*Theory Division, Saha Institute of Nuclear Physics, HBNI, Kolkata-700064, India*

²*School of Physical Sciences, National Institute of Science Education and Research, HBNI, Jatni 752050, India*

(Dated: December 9, 2021)

We investigate the impact of site dilution by setting the on-site repulsion strength (U) to zero at a fraction of sites in the half-filled Hubbard model on a simple cubic lattice. We employ a semi-classical Monte-Carlo approach first to recover the zero dilution (undiluted $x = 1$) properties, including U dependence of insulator to metal crossover temperature scale T^* and long-range staggered antiferromagnetic ordering temperature (T_N). For the non-perturbative regime of $U \sim$ bandwidth, we find a rapid suppression of T^* with reducing x from 1 to 0.7. However, T_N remains unchanged in this dilution range, showing a weakening of the insulating state but not of the magnetic order. At $x \leq 0.7$, T^* and T_N coincide and are suppressed together with further increase in site-dilution. Finally, the system loses the magnetic order and the insulating state for $x = 0.15$, significantly below the classical percolation threshold $x_p^{sc} (\sim 0.31)$. We show that the induced moments on $U = 0$ sites drive the magnetic order below the classical percolation limit by studying local moment systematics and finite-size analysis of magnetic order. At the end, we show that either increasing U to large values or raising temperature beyond a U dependent critical value, suppresses the induced local moments of the $U = 0$ sites and recovers the classical percolation threshold.

I. INTRODUCTION

The discovery of high-temperature superconductivity in doped copper oxides generated an enormous amount of interest in quantum antiferromagnets¹⁻³. The emergence and collapse of long-range antiferromagnetic (AF) order, which provides us a unique way to explore many exotic magnetic phases, is one of the most essential and well-explored topics in condensed matter physics. The AF ordering in cuprate, iron-pnictide, and iron-chalcogenides gets suppressed by doping non-magnetic impurities⁴⁻⁶. Spin-wave theory for low concentration of impurities with the impurities treated as static vacancies^{7,8} can usually model such behavior. On the other hand, frustration arising from in-plane couplings in clean systems can also disrupt long-range magnetic order (LRO) and are routinely explored within the $J_1 - J_2$ Heisenberg spin models⁹⁻¹¹. Disorder-induced suppression of long-range magnetic order^{12,13} have been typically studied in the strong-coupling limit. Quantum Monte Carlo simulations¹⁴ in the large correlation strength limit, agree with the AF order vanishing at the classical percolation threshold as in the experiments.

Cuprates like $\text{La}_2\text{Cu}_x\text{Mg}_{1-x}\text{O}_4$ ¹⁵⁻¹⁸ have inspired some site-diluted Hubbard model studies in two and quasi-two dimensions¹⁹⁻²¹. The experimental motivation was to investigate superconductivity in the parent material (La_2CuO_4) by doping with non-magnetic Zn or Mg that suppresses long-range antiferromagnetic order. According to the current understanding this quasi-two dimensional material [$\text{La}_2\text{Cu}_x(\text{Mg}/\text{Zn})_{1-x}\text{O}_4$]

shows complete suppression of long-range AF order¹⁸ for $x_p^{2D} \sim 0.59$, the classical percolation threshold^{14,22}. In the strong interaction limits for such materials where $3d$ transition metal elements are involved^{14,23-25}, the long-range magnetic order vanishes at x_p , the critical classical percolation threshold in the relevant dimensions.

However, investigations of site dilution for the Hubbard model where U is comparable to bandwidth (BW) are relevant both for materials and is of theoretical interest. In particular, since the correlation-induced suppression of double occupation is not too severe, sites with $U = 0$ in vicinity of $U \neq 0$ sites can get effected by virtual charge fluctuations leading to induced moments on the uncorrelated sites. Thus, whether site dilution will suppress the long-range antiferromagnetic order of the undiluted system is unclear. A recent study of the diluted Hubbard model on Lieb lattice shows that magnetic order is very robust for dilution much lower than the classical percolation threshold²⁶.

In this paper, we analyze the effect of site dilution in a Hubbard model at half-filling using a semi-classical Monte-Carlo scheme (s-MC)^{27,28}. The method reduces to an unrestricted Hartree-Fock method at very low temperatures but becomes progressively accurate with temperature increase and, in particular, compares well with Determinant Quantum Monte Carlo (DQMC) over a wide temperature range. We consider the half-filled Hubbard model as defined below in three dimensions. We first produce several benchmarks for the undiluted case, including the AF magnetic order. We then show that switching off interaction potential on a fraction of sites weakens and eventually destroys the magnetic order. However, remarkably, for correlation strength, where the bandwidth (BW) and interaction strength (U) are comparable, we show that the AF order survives to dilutions much below the classical percolation threshold. We investigate this

*anamitra@niser.ac.in

†kalpataru.pradhan@saha.ac.in

phenomenon by tracking the local moment dependence with temperature. We show that $U \neq 0$ sites induce significant suppression of double occupation on the $U = 0$ sites stabilizing local moments on the uncorrelated sites. In addition our calculations reveal that the density of states carries the signature of this effect and manifests as a four-lobe Mott insulator. At a critical dilution below the classical threshold, we show that the collapse of local moments at the $U = 0$ sites signals the onset of a metallic state. We find that the ensuing metal has a pseudo-gapped density of states at low temperatures. We characterize the percolative metallic state and its temperature dependence. Finally, we demonstrate that the vanishing of the AF order at the classical percolation threshold occurs for U much larger than the BW, in agreement with earlier literature. We also find that the same can happen at increased temperatures where thermal fluctuations destroy the local moments on the $U = 0$ sites. Thus we present a complete phenomenology within our semi-classical approach of site dilution effects, correlation strength, and temperature.

II. MODEL & METHOD

We consider the following particle-hole symmetric form of the one band Hubbard Hamiltonian:

$$H = -t \sum_{\langle i,j \rangle, \sigma} (c_{i\sigma}^\dagger c_{j\sigma} + h.c.) + U \sum_i \left(n_{i\uparrow} - \frac{1}{2} \right) \left(n_{i\downarrow} - \frac{1}{2} \right) - \mu \sum_i n_i \quad (1)$$

where $c_{i\sigma}$ ($c_{i\sigma}^\dagger$) are the fermion annihilation (creation) operators at site i with spin σ . t is the nearest neighbor hopping parameter and U (> 0) denotes the on-site repulsive Hubbard interaction. μ is the chemical potential.

To employ the s-MC approach we decompose the on-site interaction term by introducing standard Hubbard-Stratonovich (HS) auxiliary fields (a vector field m_i that couples to spin degrees of freedom while a scalar field ϕ_i couples to charge degree of freedom) at each site i . We treat auxiliary fields as *classical fields* by dropping the time dependence explicitly. We treat ϕ_i at the saddle point level $i\phi_i = \frac{U}{2} \langle n_i \rangle$, but retain the thermal fluctuations for m_i . These thermal fluctuations are necessary to capture many of the well established features which will be discussed later. The following effective spin-fermion Hamiltonian is derived using above approximations (see supplementary materials for the details and justification of the approximation):

$$H_{eff} = -t \sum_{\langle i,j \rangle, \sigma} (c_{i\sigma}^\dagger c_{j\sigma} + h.c.) + U/2 \sum_i (\langle n_i \rangle n_i - \mathbf{m}_i \cdot \boldsymbol{\sigma}_i) + (U/4) \sum_i (\mathbf{m}_i^2 - \langle n_i \rangle^2) - \frac{U}{2} \sum_i n_i - \mu \sum_i n_i$$

The chemical potential is varied to maintain the system at half filling. We solve H_{eff} by using exact diagonalization based Monte-Carlo method. We diagonalize the Hamiltonian

for a fixed set of $\{\mathbf{m}_i\}$ and $\{\langle n_i \rangle\}$ configuration. We update the $\{\mathbf{m}_i\}$ at each site based on usual Metropolis scheme at a fixed temperature. The $\langle n_i \rangle$ fields are self consistently updated at every 10^{th} Monte-Carlo step where the \mathbf{m}_i fields are held fixed. The goal of the process is to generate equilibrium configuration of the \mathbf{m}_i and the $\langle n_i \rangle$ fields. Expectation values of observables are obtained by appropriately using the eigenvectors and eigenvalues resulting from diagonalizing the Hamiltonian in each of the equilibrium configuration. These individual expectation values from equilibrium configurations are further averaged over results from 100 such configurations at a fixed temperature. All observables are calculated at a given temperature by averaging over the values obtained from individual configurations. We note that we calculate observables from every tenth equilibrium configuration to avoid spurious self correlations. Temperature is lowered in small steps to allow for equilibration. To avoid size limitation we employ above mentioned Monte-Carlo technique within a traveling cluster approximation²⁹⁻³¹ to handle system size $N = L^3 = 10^3$.

For $0 < x < 1$, we have Nx fraction of sites with finite U and $N(1-x)$ sites with $U = 0$, with N being the total number of sites. For $U = 8$, on-site interactions (U_i) at each sites are chosen using the distribution $P(U_i) = (1-x)\delta(U_i) + x\delta(U_i - 8)$. We introduce the HS auxiliary fields only on the $U \neq 0$ sites. The induced moments on the $U = 0$ sites are calculated by computing quantum local moments as we discuss later. Finally, all energy scales (U , temperature, BW etc.) are measured in units of the hopping parameter t .

III. PHASE DIAGRAM

First we discuss briefly about the $U-T$ phase diagram, seen in the inset of Fig. 1, obtained for $x=1$ (i.e. the undiluted case, without any $U=0$ sites). We first find that for all U , we have a staggered AF insulating ground state (AF-I). The staggered AF transition temperature T_N defines the finite temperature boundary of the AF and the PM phase. The antiferromagnetic transition temperature T_N increases with U up to $U=8$ and decreases thereafter. For larger U s-MC captures $\sim t^2/U$ scaling of T_N . In the inset we also find that for large U , above T_N , there is an insulating region of preformed local moments with no long range magnetic order (PM-I). This phase crosses over to a paramagnetic metal (PM-M) above the dashed line. We discuss below how these phases are determined for different values of x . For the $x = 1$ case, the non-monotonic U dependence of T_N and the preformed local moment regime at finite temperature are results beyond simple finite temperature Hartree-Fock mean field theory. Details and comparison with DQMC are presented in earlier s-MC literature²⁷. s-MC has also been used to study the physics of Anderson-Hubbard model³² and frustrated Hubbard model^{33,34}.

As mentioned in the introduction, our main motivation is to examine if the AF order can survive below the classical percolation threshold. For this we initially confine to $U = 8$ where T_N is optimum and study the effect of site-dilution. This value of U is away from the two perturbative limits of $U/BW \ll 1$ and $U/BW \gg 1$. We will discuss the systematics of varying U at a later stage. The main panel in Fig. 1, shows the $x-T$ phase diagram for $U = 8$. We see that the T_N (diamonds) and crossover scale (dashed line) both decrease as x is reduced. Within numerical accuracy, the PM-I phase ex-

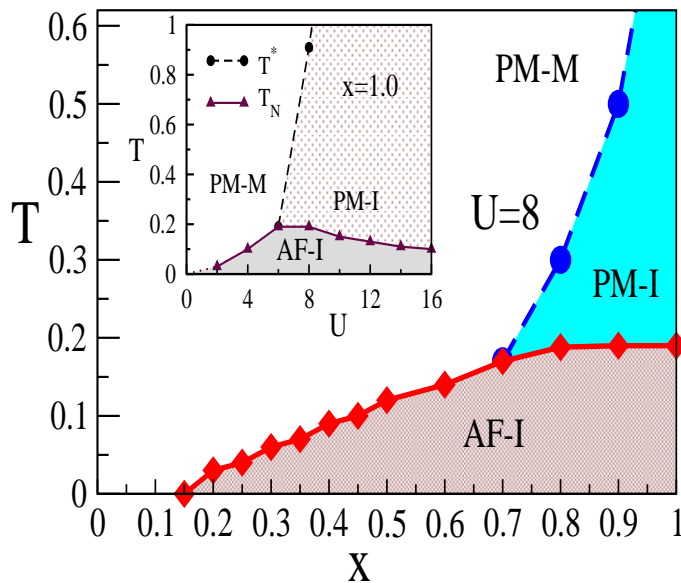


FIG. 1: $x-T$ phase diagram for $U=8$. x is the concentration of correlated sites ($U=8$) and rest of the sites (with concentration $1-x$) have $U=0$. PM-I phase intervenes between the PM-M and AF-I phase for $x > 0.7$. For $x \leq 0.7$ the PM-I phase vanishes and the metal insulator transition coincides with the onset of the AF order. For $x \leq 0.15$ the AF order completely collapses at low temperatures. The inset shows the $U-T$ phase diagram. For details please see the text.

ists for $x > 0.7$. The important observation is that the T_N survives up to $x = 0.15$, much smaller than the classical three dimensional percolation threshold ($x_p^{sc} \sim 0.31$). We will show below that this conclusion is robust to changes in the system size.

IV. MAGNETIC AND TRANSPORT PROPERTIES

Next we discuss the magnetic and transport properties in details that we used to construct the phase diagram for site-diluted Hubbard model (Fig. 1).

Metal-insulator transition & magnetic order: From the $x=1$ analysis we know that local moments exist on all sites for $U=8$. For $x=1$ the system averaged quantum local moment is defined as $M = \langle (n_\uparrow - n_\downarrow)^2 \rangle = \langle n \rangle - 2\langle n_\uparrow n_\downarrow \rangle$, where the angular brackets imply quantum and thermal averaging at individual sites. The large moment at low temperature is due to the increased suppression of doublons (local double occupation). In the limit $U \rightarrow \infty$ and any finite temperature we expect the double occupation to go to zero giving $M=1$. In the other extreme limit of $U=0$ or $T \rightarrow \infty$ at any finite U , the double occupation $\langle n_\uparrow n_\downarrow \rangle \rightarrow \langle n_\uparrow \rangle \langle n_\downarrow \rangle = 0.25$. This gives the value of M to be 0.5. In Fig. 2 (a) main panel we show the local moment M vs temperature data for various x values for the $U \neq 0$ sites. For $x=1$, this of course coincides with the system averaged local moments, while for $x \neq 1$, the site averaging is done only over the $U \neq 0$ sites.

To understand the actual temperature scale for moment

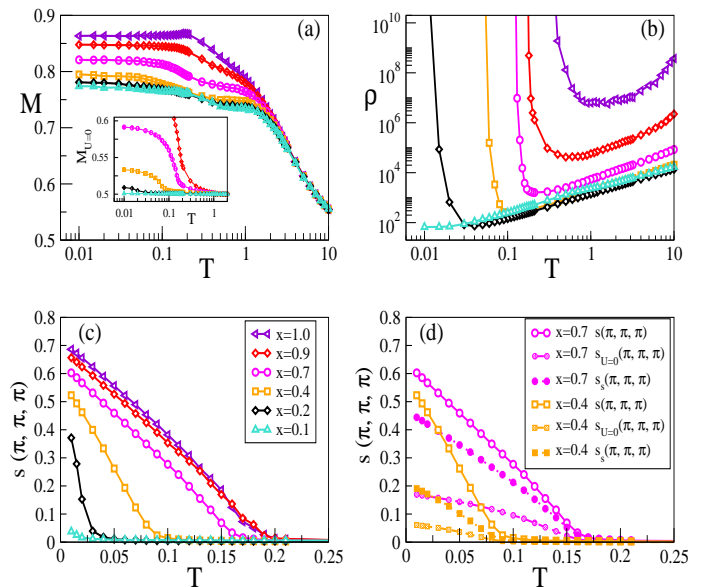


FIG. 2: Physical quantities for different x values. All calculations are done for $U=8$ unless otherwise specified. (a) Average local moments M vs temperature measured using only $U=8$ sites. Inset shows the induced moments with temperature at $U=0$ sites. Legends are same in (a)-(c). (b) Resistivity vs temperature curves for different x values. (c) $s(\pi, \pi, \pi)$ vs temperature (by taking $U=8$ sites only) for different x . With decrease in x the quantum structure factor decreases at low temperature. T_N also decreases and vanishes for $x=0.1$. (d) $s_s(\pi, \pi, \pi)$, structure factor for taking both $U=0$ and $U=8$ sites, vs temperature shows that the system as a whole turns antiferromagnetic at the same temperature to that of $U=8$ sites. For comparison $s_{U=0}(\pi, \pi, \pi)$, calculated only for $U=0$ sites for specific x are also shown.

formation that lies between these two limits and its impact on transport properties we calculate the resistivity as function of temperature in Fig. 2(b). Resistivity is calculated for different x values by calculating the dc limit of the optical conductivity determined by the Kubo-Greenwood formula^{35,36}. A metal to insulator crossover (MIC) scale (T^*) is ascertained from the sign of $d\rho/dT$. For $x=1$, and $U=8$, $T^* \sim 1$. For the $x < 1$ case we see that this crossover scale reduces rapidly. In order to understand this systematically, in (a) we plot the local moments of the correlated ($U \neq 0$) and uncorrelated ($U=0$) sites separately. For the correlated sites we see that there is an overall reduction in the local moment magnitudes, but there is no drastic local moment collapse to suggest a significantly smaller MIC temperature as the resistivity data suggests. However, the remarkable effect on deciding the scale for onset of metallicity with temperature increase comes from the $U=0$ sites! In the inset of (a), we see that weak local moments are induced on the uncorrelated sites. We observe that T^* is controlled by the onset temperature of the local moments formation (M becoming greater than 0.5) on the uncorrelated sites. For example for $x=0.9$, the local moments of the correlated sites are similar in magnitude to the $x=1$ case, yet the resistivity data shows an insulator to metal crossover occurs at $T^* \sim 0.5$ as opposed to ~ 1 for $x=1$ case. Interestingly the onset of magnetic moments on

$U = 0$ sites, transition from PM-M to AF-I phase occurs at same temperature for $x \leq 0.7$. This clear correlation needs the following clarification: whether the small moments on the $U = 0$ sites, for example small moments very close to the uncorrelated value of 0.5, for $x < 0.4$, responsible for stabilizing the low temperature antiferromagnetic insulating state? In particular, is there a long range order arising out of the sites with two values of moments?

To answer this question, in (c) we plot the quantum antiferromagnetic correlations $s(\pi, \pi, \pi)$ [$s(\mathbf{q}) = \frac{1}{(Nx)^2} \sum_{mn} \langle \mathbf{s}_m \cdot \mathbf{s}_n \rangle e^{i\mathbf{q} \cdot (\mathbf{r}_m - \mathbf{r}_n)}$ where \mathbf{q} is the wave vector], where angular brackets have the same meaning as mentioned above and the indices $\{m, n\}$ run over only the $U = 8$ sites. The normalization is defined accordingly. The reduction in the T_N as well as the low T saturation value with decreasing x is apparent. The weakening of antiferromagnetism due to site dilution is expected. However, we find an unexpected behavior when comparing the above with magnetic structure factor computed only for the $U = 0$ sites [denoted as $s_{U=0}(\pi, \pi, \pi)$]. In (d) we show two such comparisons at the indicated values of x . The AF order that results from the $U = 0$ sites by itself generates long range staggered AF correlations in three dimensions. Further, the AF order from the two set of sites (taking $U=8$ and $U=0$ sites separately) and AF correlations $s_s(\pi, \pi, \pi)$ obtained by taking all the sites (both $U=8$ and $U=0$ sites at the same time) vanish at the same temperature. This shows cooperation of the $U \neq 0$ and $U = 0$ matrix. In addition, for $x \leq 0.7$, we find that the insulating state and the T_N coincide, reminiscent of a Slater like insulator. However, unlike the Slater insulator, this is clearly not arising out of a nesting instability. For $x > 0.7$, the data suggests that the insulating state can survive without the magnetic order, but requires finite local moments at the $U = 0$ sites. This is the continuation of the $x = 1$ PM-I phase for $x < 1$.

Density of states: In Fig. 3 (a) we show the temperature evolution of the density of states at the chemical potential $N(\omega = \mu)$ for different values of x . Density of states are obtained by implementing the Lorentzian representation of the δ function in $N(\omega) = \sum_k \delta(\omega - \omega_k)$, where ω_k are the eigenvalues of the fermionic sector and the summation runs up to $2L^3$, i.e. the total number of eigenvalues of a L^3 system. The expected gradual filling up of the charge gap in the Mott state seen for $x = 1$ as also seen in³⁷ for smaller x values. The gap filling however becomes abrupt for $x \leq 0.7$. This is the same dilution below which we have a direct transition from a PM-M to an AF-I. In addition, the density of states are plotted explicitly for $x = 0.7$, in Fig. 3(b) at different temperatures. While not explored herein detail, overall the data suggests a possible first order transition for $x \leq 0.7$. Finally for $x = 0.1$, we have a gap-less ground state.

The density of states are compared for different x values at low temperature $T = 0.02$, in Fig. 3(c). We see that with reducing x , the upper and lower Hubbard sub-bands around $\pm U/2$ evolves in to a four sub-band structure and the gap around chemical potential μ ($\omega=0$) reduces. The gap eventually closes and we find a pseudo-gapped metal for $x = 0.1$. To understand the origin of the new features in the density of states we show the contribution of the DOS from $U = 0$ and $U = 8$ sites separately in panel (d) for $x = 0.7$ at the same low temperature. It shows that $U = 0$ sites mostly contribute to the formation of the low energy Mott lobes (around $\omega = \pm 1$). This four sub-band DOS within s-MC qualitatively agrees with DQMC¹⁹.

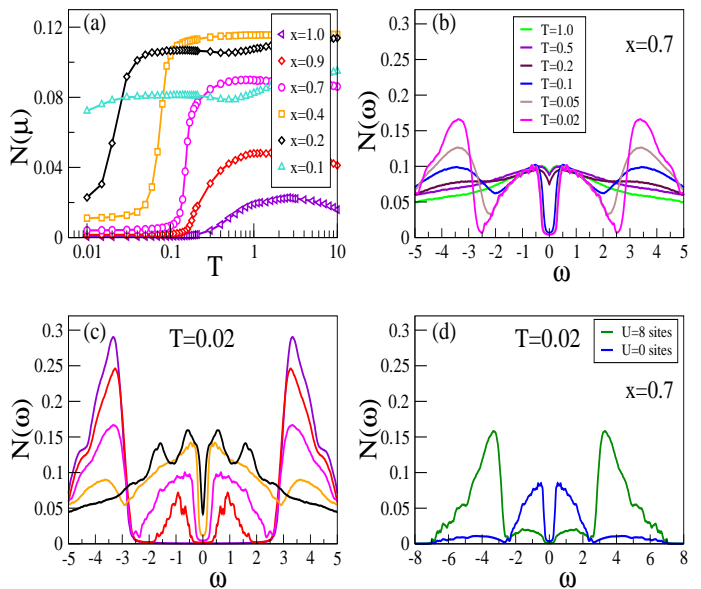


FIG. 3: (a) Temperature dependence of density of states at the Fermi energy $N(\mu)$ shows that the Mott gap collapses at high temperature due to thermal fluctuation. Thermal fluctuation persists up to low enough temperature for lower x values. $N(\mu)$ more or less remains constant with temperature for $x = 0.1$. (b) Density of states $N(\omega)$ with ω for different temperatures at $x = 0.7$. (c) Density of states $N(\omega)$ with ω for different x at $T = 0.02$. Legends are same in (a) and (c). For $x = 1$, the Mott gap at $T = 0.02$ show Mott lobes around $\pm U/2$. A pair of secondary Mott lobe forms near $\omega = 0$ for $x < 1$. (d) U dependent density of states for $x = 0.7$ shows that the secondary lobes are mainly due to the $U = 0$ sites.

V. PERCOLATION THRESHOLD

To start with, we first demonstrate the stability of the critical percolation threshold obtained from finite size lattices. Since the AF order parameter is the central indicator used by us, in Fig. 4 we show the low temperature value of $s(\pi, \pi, \pi)$ for different system sizes as a function of x . The system size is defined as L^3 . Beyond 10^3 the results for low x are barely distinguishable from each other. We see from the data that the order parameter rapidly converges with system size, giving the limiting value of $x_p = 0.15$. The inset(i) shows $s(\pi, \pi, \pi)$ plotted as a function of inverse system size ($1/L$) for three values of x . We find the for $x > 0.15$, $s(\pi, \pi, \pi)$ saturates to a finite value for $L \rightarrow \infty$, while it approaches zero for $x = 0.15$. This analysis shows that indeed in the thermodynamic limit the AF order survives below the classical percolation threshold $x_p^{sc} \sim 0.31$. Inset(ii) shows that the long range AF order also persists up to $x=0.15$ for $T = 0.01$.

In order to clarify the nature of the antiferromagnetic order below the $x_p^{sc} \sim 0.31$, in Fig. 5(a) we present the distribution of local moments in real space that includes both the $U = 0$ and $U = 8$ sites at $T = 0.02$. The local moment distribution $P_q(M) = \sum_{M_i} \delta(M - M_i)$ show two peaks. In the limiting case of $x = 1$ the expected plot is that of a single peak at $M = 0.86$, implying uniform local moment magnitudes on all sites within the semi-classical calculation. As x is reduced, a new peak at lower M appears that indicates the moment

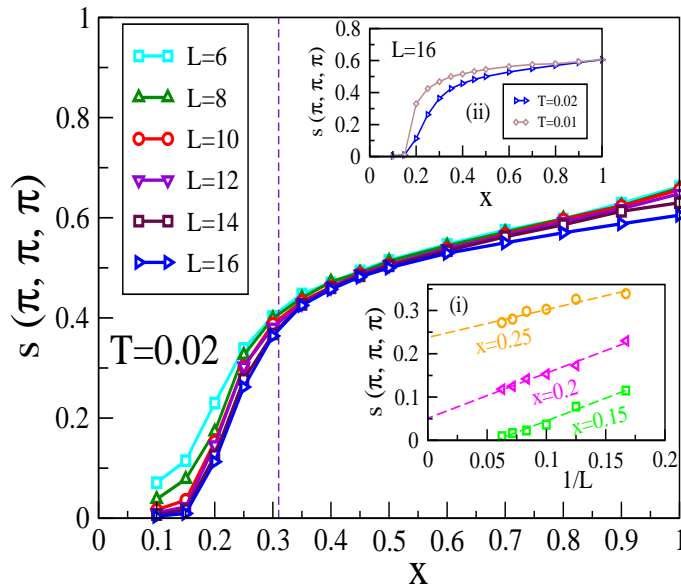


FIG. 4: Shows the drop of $s(\pi, \pi, \pi)$ with decrease in x values for different L values ($N=L^3$). For $T = 0.02$ long range AF order persists up to $x=0.15$. This AF order is due to the induced moment formed at $U = 0$ sites as explained in the text. The result is almost indistinguishable beyond system size 10^3 . All calculations are done for $U = 8$. Inset(i) shows the $s(\pi, \pi, \pi)$ vs $1/L$ for $x = 0.15, 0.2$ and 0.25 . Inset also shows linear fitting of $s(\pi, \pi, \pi)$ with $1/L$ for $x = 0.15, 0.2$ and 0.25 . Inset(ii) shows that the long range AF order also persists up to $x=0.15$ for $T = 0.01$.

formation at $U = 0$ sites. Inset of Fig. 5(a) for $x = 0.4$ confirms this scenario. This also corroborates the data shown in the inset of Fig. 2 (a) that shows the signature of induced moment on the uncorrelated ($U = 0$) sites. Just as seen in Fig. 2 (a), here too we see that if the x reduces, the location of the new peak moves towards $M = 0.5$ signaling that the induced moment magnitudes get weaker. In addition, we note that the increase in the peak height at low M is simply due to increasing number of $U = 0$ sites as x approaches zero.

Correlating the low temperature induced M in the $U = 0$ sites with the AF order parameter in Fig. 5(b), we see a crucial fact that the long range AF order between $U = 8$ sites depends on the existence of local moments at $U = 0$ sites. Induced moment at $U = 0$ sites are almost zero up to $x = 0.15$ and the system remains paramagnetic. Beyond $x = 0.15$ the induced moment at $U = 0$ sites increase and as a result the system enters into an antiferromagnetic state at small x . This intimate relation between long range AF order and induced moments in the $U = 0$ sites is central to the stability of the AF order below the classical percolation threshold. Above $x \sim 0.31$, while the cooperation continues to exist as discussed in context of Fig. 2 (d), the AF order can stabilize by the usual percolation mechanism as well.

We now analyze the recovery of the classical percolation threshold in two cases, (i) at relatively large temperature and (ii) at high U values. In Fig. 5(c) we show the AF order parameter as function of x at three different temperatures. While there is an overall suppression of the order parameter magnitude with temperature, importantly we see that the

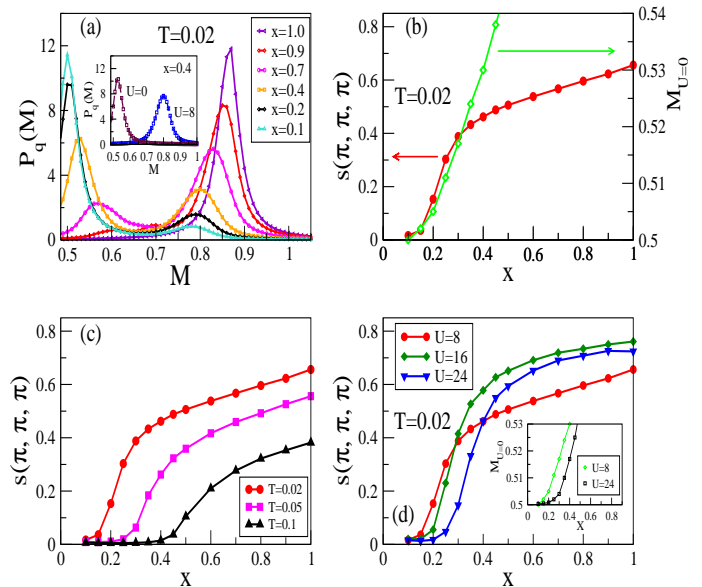


FIG. 5: (a) Distribution of local moments at $U = 8$ and $U = 0$ sites for different x values; the peak around $M = 0.8$ is for the finite U sites whereas peak at lower M is for the induced moments ($M_{U=0}$) at $U = 0$ sites. Inset shows the distribution for $U = 0$ and $U = 8$ sites separately at $x = 0.4$. (b) $s(\pi, \pi, \pi)$ and induced moment ($M_{U=0}$) at $U = 0$ sites with x for $T = 0.02$ shows one to one correspondence with the onset of antiferromagnetic correlations and formation in induced magnetic moments at $U = 0$ sites. The induced moments mediate the antiferromagnetic correlation below classical percolation threshold limit. (c) $s(\pi, \pi, \pi)$ vs x for different temperatures show that the percolation threshold increases with temperature. (d) $s(\pi, \pi, \pi)$ vs x for different U values at $T = 0.02$. The percolation threshold increases with U values due to suppression of charge fluctuations at large U . The inset shows comparison of the induced moment ($M_{U=0}$) at $U = 0$ sites with x between $U = 8$ and $U = 24$.

critical threshold of x for sustaining AF order moves towards the x_p^{sc} . The increase in temperature, disrupts the local moment order for the $U = 0$ sites, as was also seen from the smaller charge gap in the DOS shown in Fig. 3 (c). Thus the system approaches the classical threshold for maintaining long range AF order. The percolation threshold x_p also increases with U as shown in Fig 5(d). It is known that at large U the charge fluctuations are suppressed and the Hubbard model is well described by the Heisenberg Model. The induced magnetic moment that mediates the antiferromagnetism below x_p^{sc} values (for example induced moments at $U=0$ sites for $x=0.2$ and $U = 8$ case) are not induced at larger U values [see the inset of Fig 5(d)] due to suppression of spin fluctuations. As a result the x_p increases with U .

VI. CONCLUSIONS

We have employed a semi-classical technique to map out the temperature vs dilution phase diagram of the ‘diluted Hubbard model’. Our results at low temperature is close to unrestricted Hartree-Fock method and become progres-

sively accurate with temperature. Within this scheme we have shown that away from the weak coupling ($U \ll BW$) and strong coupling ($U \gg BW$) limit, site dilution weakens the long range magnetic order, but allows it to survive to dilution values much below the classical percolation threshold. At low temperature, the Mott insulator at $x = 1$ evolves in to pseudo-gapped metal (for $x \leq 0.15$) by non-trivial spectral weight transfer phenomena that transforms the two Mott sub-bands into four sub-bands. Our analysis shows that in this regime the system has two distinct energy scales for charge excitations, one controlled by U and another emergent gap that arises out of weak local moment induced on the $U = 0$ sites. Such behavior of DOS qualitatively agrees with DQMC studies in two dimensions¹⁹. By performing finite size scaling analysis, we also show that the induced moments at the $U = 0$ sites and the $U \neq 0$ sites cooperate to form long range magnetic order in the thermodynamic limit. We further demonstrate that cooperation between the $U = 0$ and $U \neq 0$ sites is crucial to the magnetic order by showing that increasing U to large values, brings the critical percolation threshold to the classical value which requires system spanning AF patches exclusively made out of $U \neq 0$ sites. In addition by increasing temperature we have shown that the closure of the Mott gap by closing the smaller charge gap again disrupts the cooperation between the AF order between the two kinds of sites which pushes the percolation threshold to the classical values. This phenomenology is also seen in exact diagonalization where local Kondo coupling and RKKY scales compete to control the magnetic properties of $s - d$ models for carbon nanotubes³⁸ and broadly agrees with DQMC study on Lieb lattice²⁶.

VII. SUPPLEMENTARY INFORMATION

We consider the following electron-hole symmetric (EHS) one band Hubbard Hamiltonian:

$$H = -t \sum_{\langle i,j \rangle, \sigma} c_{i,\sigma}^\dagger c_{j,\sigma} + U \sum_i \left(n_{i,\uparrow} - \frac{1}{2} \right) \left(n_{i,\downarrow} - \frac{1}{2} \right)$$

where ‘ t ’ is the nearest neighbor hopping parameter and ‘ U ’ denotes the on-site Hubbard interaction. We set $t=1$ in our calculations.

After some trivial algebra and dropping a constant term the EHS Hubbard model becomes:

$$H = -t \sum_{\langle i,j \rangle, \sigma} c_{i,\sigma}^\dagger c_{j,\sigma} + U \sum_i n_{i,\uparrow} n_{i,\downarrow} - \frac{U}{2} \sum_i n_i$$

We denote the nearest neighbor hopping term and the third term which is a one body operator as H_0 and the second term which is the interaction term as H_1 . We need to transform the interaction term as a combination of two quadratic terms

to set up the Hubbard-Stratonovich (HS) decomposition formalism.

$$n_{i,\uparrow} n_{i,\downarrow} = \left[\frac{1}{4} n_i^2 - S_{iz}^2 \right] = \left[\frac{1}{4} n_i^2 - (\mathbf{S}_i \cdot \hat{\Omega}_i)^2 \right] \quad (2)$$

Here \mathbf{S}_i is the spin operator which is defined as $\mathbf{S}_i = \frac{\hbar}{2} \sum_{\alpha\beta} c_{i,\alpha}^\dagger \sigma_{\alpha,\beta} c_{i,\beta}$, $\hat{\Omega}$ is an arbitrary unit vector, σ 's are the Pauli matrices and we take \hbar to be 1. We use the rotational invariance of S_{iz}^2 i.e. $(\mathbf{S}_i \cdot \hat{\Omega}_i)^2 = S_{ix}^2 = S_{iy}^2 = S_{iz}^2$.

Partition function for the Hamiltonian is $Z = Tr e^{-\beta H}$, where β is inverse temperature ($1/T$) [k_B is set to 1]. Next we divide the interval $[0, \beta]$ into M equally spaced slices, defined by $\beta = M\Delta\tau$, separated by $\Delta\tau$ and labeled from 1 to M . For large M , $\Delta\tau$ is a small parameter and allows us to employ the Suzuki-Trotter decomposition, so that we can write $e^{-\beta(H_0+H_1)} = (e^{-\Delta\tau H_0} e^{-\Delta\tau H_1})^M$ to first order in $\Delta\tau$. Then using Hubbard-Stratonovich identity $e^{-\Delta\tau U [\sum_i \frac{1}{4} n_i^2 - (\mathbf{S}_i \cdot \hat{\Omega}_i)^2]}$ can be shown to be proportional to,

$$\int d\phi_i(l) d\Delta_i(l) d^2\Omega_i(l) \times e^{-\Delta\tau [\sum_i (\frac{\phi_i^2}{U} + i\phi_i(l)n_i + \frac{\Delta_i^2}{U} - 2\Delta_i(l)\hat{\Omega}_i(l)\mathbf{S}_i)]}$$

Here $\phi_i(l)$ is the auxiliary field for charge density and $\Delta_i(l)$ is auxiliary field for spin density and ‘ (l) ’ is a generic time slice. Further we define a new vector auxiliary field \mathbf{m}_i as the product of $\Delta_i(l)\hat{\Omega}_i(l)$. Putting all of this back to the partition function we find the effective Hamiltonian. Now we make two approximations which make our model different from DQMC. Firstly we drop the τ dependence of the Hamiltonian and we use the saddle point value of $i\phi_i = \frac{U}{2} \langle n_i \rangle$. Lastly by rescaling $\mathbf{m}_i \rightarrow (U/2)\mathbf{m}_i$ we find the effective Hamiltonian as:

$$H_{eff} = -t \sum_{\langle i,j \rangle, \sigma} c_{i,\sigma}^\dagger c_{j,\sigma} + U/2 \sum_i (\langle n_i \rangle n_i - \mathbf{m}_i \cdot \sigma_i) + (U/4) \sum_i (\mathbf{m}_i^2 - \langle n_i \rangle^2) - \frac{U}{2} \sum_i n_i - \mu \sum_i n_i$$

The chemical potential μ is used to tune the global electron density equal to 1. In our calculation we have considered finite U at randomly chosen sites k with a concentration x and $U = 0$ at rest of the sites (concentration $1 - x$). So, we consider following diluted Hamiltonian for our calculations:

$$H_{eff} = -t \sum_{\langle i,j \rangle, \sigma} c_{i,\sigma}^\dagger c_{j,\sigma} + U/2 \sum_k (\langle n_k \rangle n_k - \mathbf{m}_k \cdot \sigma_k) + (U/4) \sum_k (\mathbf{m}_k^2 - \langle n_k \rangle^2) - \frac{U}{2} \sum_k n_k - \mu \sum_i n_i$$

Acknowledgment: We acknowledge use of Meghnad2019 computer cluster at SINP.

¹ P. W. Anderson, Science **235**, 1196 (1987).

² S. Sachdev, Nature Phys. **4**, 173 (2008).

³ B. Keimer, S. A. Kivelson, M. R. Norman, S. Uchida, and

J. Zaanen, Nature (London) **518**, 179 (2015).

⁴ T. J. Liu *et al.*, Nat. Mater. **9**, 718 (2010).

⁵ C.-W. Liu, S. Liu, Y.-J. Kao, A. L. Chernyshev, and A.

- W. Sandvik, Phys. Rev. Lett. **102**, 167201 (2009).
- ⁶ M. R. Norman, Physics **1**, 21 (2008).
 - ⁷ M. Kircan and M. Vojta, Phys. Rev. B **73**, 014516 (2006).
 - ⁸ A. L. Chernyshev, Y. C. Chen, and A. H. Castro Neto, Phys. Rev. Lett. **87**, 067209 (2001).
 - ⁹ M. Sato, S. Furukawa, S. Onoda, A. Furusaki, Mod. Phys. Lett. B **25**, 901 (2011).
 - ¹⁰ L. Wang and A. W. Sandvik, Phys. Rev. Lett. **121**, 107202 (2018).
 - ¹¹ B. Schmidt and P. Thalmeier, Phys. Rep. **703**, 1 (2017).
 - ¹² Y. H. Szczech, M. A. Tusch, and D. E. Logan, J. Phys.: Condens. Matter **10**, 639 (1998).
 - ¹³ S. Singh Kunwar, A. Sen, T. Vojta, and R. Narayanan, Phys. Rev. B **98**, 024206 (2018)
 - ¹⁴ A. W. Sandvik, Phys. Rev. B **66**, 024418 (2002).
 - ¹⁵ A. Chakraborty, A. J. Epstein, M. Jarrell, and E. M. McCarron, Phys. Rev. B **40**, 5296(R) (1989).
 - ¹⁶ S. W. Cheong, A. S. Cooper, L. W. Rupp, B. Batlogg, J. D. Thompson, and Z. Fisk, Phys. Rev. B **44**, 9739(R) (1991).
 - ¹⁷ C. C. Wan, A. B. Harris, and J. Adler, J. Appl. Phys. **69**, 5191 (1991).
 - ¹⁸ O. P. Vajk, P. K. Mang, M. Greven, P. M. Gehring, and J. W. Lynn, Science **295**, 1691 (2002).
 - ¹⁹ M. Ulmke, P. J. H. Denteneer, R. T. Scalettar, and G. T. Zimanyi, Europhys. Lett. **42**, 655 (1998).
 - ²⁰ A. Medhi, S. Basu, and C. Kadolkar, Journal of App. Phys. **101**, 09D504 (2007).
 - ²¹ J.-Y. P. Delannoy, A. G. Del Maestro, M. J. P. Gingras, and P. C. W. Holdsworth, Phys. Rev. B **79**, 224414 (2009).
 - ²² K. Christensen, Percolation theory, Imperial College London (2002).
 - ²³ K. Kato, S. Todo, K. Harada, N. Kawashima, S. Miyashita, and H. Takayama Phys. Rev. Lett. **84**, 4204 (2000).
 - ²⁴ A. L. Chernyshev, Y. C. Chen, and A. H. Castro Neto, Phys. Rev. B **65**, 104407 2002.
 - ²⁵ P. Carretta, G. Prando, S. Sanna, R. De Renzi, C. Decorse, and P. Berthet, Phys. Rev. B **83**, 180411(R) (2011).
 - ²⁶ L. Oliveira-Lima ,N. C. Costa ,J. Pimentel de Lima, R. T. Scalettar, and R. R. dos Santo, Phys. Rev. B **101**, 165109 (2020).
 - ²⁷ A. Mukherjee, N. D. Patel, S. Dong, S. Johnston, A. Moreo, and E. Dagotto, Phys. Rev. B **90**, 205133 (2014).
 - ²⁸ A. Mukherjee, N. D. Patel, C. Bishop, and E. Dagotto Phys. Rev. E **91**, 063303 (2015).
 - ²⁹ S. Kumar and P. Majumdar, Eur. Phys. J. B **50**, 571 (2006).
 - ³⁰ K. Pradhan and S. Yunoki, Phys. Rev. B **96**, 214416 (2017).
 - ³¹ S. Chakraborty, S.K. Das, and K. Pradhan, Phys. Rev. B **102**, 245112 (2020).
 - ³² N. D. Patel, A. Mukherjee, N. Kaushal, A. Moreo, and E. Dagotto Phys. Rev. Lett. **119**, 086601 (2017).
 - ³³ G. Jana and A. Mukherjee, J. Phys.: Condens. Matter **32** 365602 (2020).
 - ³⁴ R. Tiwari and P. Majumdar, Europhysics Letters **108**, 27007 (2014).
 - ³⁵ G. D. Mahan, *Quantum Many Particle Physics* (Plenum Press, New York, 1990).
 - ³⁶ S. Kumar and P. Majumdar, Europhys. Lett. **65**, 75 (2004).
 - ³⁷ T. Paiva, R. T. Scalettar, C. Huscroft, and A. K. McMahhan, Phys. Rev. B **63**, 125116 (2001).
 - ³⁸ Y. Luo, C. Verdozzi, and N. Kioussis Phys. Rev. B **71**, 033304 (2005).